Structural and Multidisciplinary Optimization (2022) 65:308
https://doi.org/10.1007/s00158-022-03397-5

RESEARCH PAPER

LatticeOPT: a heuristic topology optimization framework for thin-walled, 2D extruded lattices

Junyan He[1] · Shashank Kushwaha[1] · Diab Abueidda[2] · Iwona Jasiuk[1]

Received: 13 August 2022 / Revised: 3 September 2022 / Accepted: 6 September 2022 / Published online: 20 October 2022

Abstract

This paper introduces a purely heuristic topology optimization framework to improve specific energy absorption for thin-walled, extruded lattice structures. The framework optimizes the lattice cross section design by iteratively updating the lattice wall thicknesses. The main novelty of the work is the two novel thickness update schemes we proposed. The first update scheme is a direct statement of homogenization of wall-wise specific energy absorption, while the other scheme is based on the homogenization of a wall-wise sensitivity parameter inspired by the bi-directional evolutionary structural optimization method. Both schemes are based on the central idea of homogenization of certain field variables, which has been widely employed in previous optimization frameworks for thin-walled structures. The proposed framework has high potential because it can work directly with commercial finite element packages, and only requires information on the energy absorption of each element. Without the need for the finite element stiffness matrix, this framework can be used with explicit dynamics simulations to treat highly nonlinear problems. Three numerical examples are presented: (1) optimization of a column under axial compression, (2) optimization of a lattice-reinforced beam under dynamic three-point bending, and (3) optimization of a lattice-filled sandwich panel under blast loading. The results show that the framework can effectively increase specific energy absorption with as few as 25 nonlinear finite element simulations.

Graphical abstract

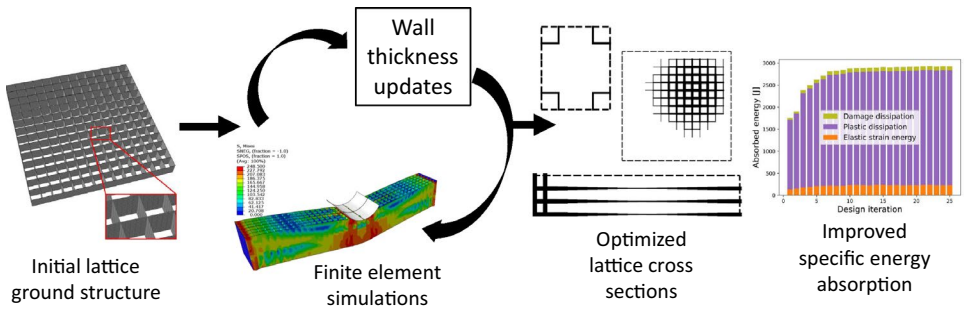

Keywords Topology optimization · Thin-walled extruded lattice · Blast loading · High strain rate loading

Responsible Editor: Makoto Ohsaki

✉ Iwona Jasiuk
ijasiuk@illinois.edu

[1] Department of Mechanical Science and Engineering, University of Illinois at Urbana-Champaign, Champaign, IL, USA

[2] National Center for Supercomputing Applications, University of Illinois at Urbana-Champaign, Champaign, IL, USA

1 Introduction

Thin-walled lattices are often employed to strengthen structures for energy absorbing purposes (Sun et al. 2010; Yin et al. 2014; San Ha and Lu 2020). Typically, these structures absorb energy by undergoing highly nonlinear large deformation that extends well beyond the linear elastic region (Duddeck et al. 2016). Irreversible processes such as plastic

deformation, damage, and fracture become the primary means of energy dissipation (Zhu et al. 2020; Baroutaji et al. 2017). It is of significant practical interest to leverage topology optimization (TO) algorithms to identify the optimum cross-sectional design and location of reinforcements (Duddeck et al. 2016). The objectives are typically to maximize specific energy absorption (SEA) (Yin et al. 2014; Fu et al. 2019; Sun et al. 2014), maximize crashing force efficiency (Zarei and Kröger 2007; Sun et al. 2014), and minimize peak crushing force (Wu et al. 2016; Abramowicz 2003). However, TO frameworks that are based on quasi-static loading, linear elastic, and small-strain finite element (FE) formulations are unsuitable in this case due to the large deformation and dynamic nature of the loading. For those that do account for geometric nonlinearity (Jung and Gea 2004; Clausen et al. 2015; Wallin et al. 2016), material plasticity (Abueidda et al. 2021; Wallin et al. 2016; Maute et al. 1998), and damage (Verbart et al. 2016; Li et al. 2017; James and Waisman 2015), an in-house implementation of the FE procedure is required, as information on the material tangent stiffness matrix and values of the internal state variables are needed in the adjoint method to compute the gradient of the objective function (Tsay and Arora 1990; Alberdi et al. 2018; Abueidda et al. 2021). However, many general-purpose FE codes, either open source or proprietary, already exist that can robustly solve large deformation nonlinear problems, and they should be leveraged whenever possible. In addition, information on the tangent stiffness matrix may not be provided by those programs, or in the case of explicit dynamic simulations, it is simply not formed. In particular, it is also noted that adjoint analysis for transient problems is complex and difficult to implement (Farrell et al. 2013) and can be as expensive as the FE analysis that is used to find the objective function value (Sigmund 2011).

Given that existing crashworthiness research widely employs commercial explicit dynamics FE codes such as Abaqus/Explicit (SIMULIA 2020) and LS-DYNA (Murray et al. 2007), it is highly relevant and of great importance to study how these codes can be coupled to TO frameworks that do not require information beyond what the commercial codes provide. In the case of TO for thin-walled structures, several frameworks have been proposed and demonstrated. Notable ones are: (1) the equivalent static load approach, which seeks a static load that generates equivalent deformation to the true dynamic load, and thus converts the problem to a quasi-static TO problem (Lee and Park 2015; Jang et al. 2012); (2) cellular automata-based approaches, which use a series of update rules to iteratively update the thickness of the shell elements defining the lattice walls (Hunkeler et al. 2013; Duddeck et al. 2016; Hunkeler 2014; Zeng and Duddeck 2017); (3) the response surface method, which seeks to approximate the true response surface of the objective function through simple functions and repeated FE simulations (Kurtaran et al. 2002; Avalle et al. 2002); and (4) various probabilistic and evolutionary methods like Bayesian optimization (Liu et al. 2019a), ant colony method (Liu et al. 2019b, 2021), and particle swarm method (Gao et al. 2019). Most of these methods, although capable of improving the design, take many FE simulations and optimization iterations to do so (Hunkeler et al. 2013), and can be computationally expensive for large-scale problems. Therefore, the current work proposes a novel heuristic framework named LatticeOPT that can work with commercial FE code to generate lattice cross-section designs to improve SEA. We emphasize that the proposed algorithm is purely heuristic; therefore it is not mathematically guaranteed that the algorithm will improve the SEA of the structure monotonically, nor does it guarantee convergence to a local optimum. However, as we shall show later, the proposed framework does improve the SEA of the structure nonetheless.

This paper is organized as follows: Sect. 2 presents an overview of the definition of the lattice design space, thickness update schemes, and the workflow of the LatticeOPT algorithm. Section 3 presents and discusses the results from three numerical examples. Section 4 summarizes the outcomes and highlights possible future works.

2 Methods

2.1 Defining the lattice design space and design variables

Currently, the LatticeOPT framework supports the definition of a cubic lattice design space, defined by the in-plane cross-section length (L) and width (W), as well as the out-of-plane height (H). Inspired by the ground structure approach (Soto and Diaz 1999), which is typically applied to TO of truss structures, we partition the in-plane cross section into smaller rectangular cells (see Fig. 1a), where each cell wall is represented by shell elements in FE simulations. The user provides the number of cells in the X- and Y-directions, denoted by N_x and

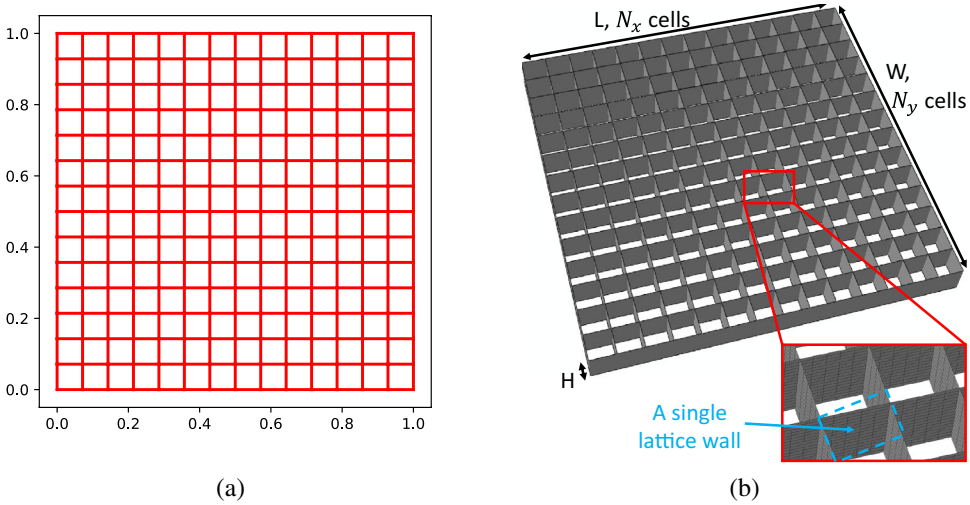

(a) (b)

Fig. 1 Design space definition: **a** The cross section is partitioned into a user-defined number of rectangular cells. Cells do not need to be squares. **b** An extruded lattice is constructed from the cross section and a user-defined height; the inset shows the finite element mesh. The length (L), width (W), and height (H) as well as the number of cells in the X- and Y-directions are also shown for clarity. The blue dashed line highlights a single cell wall, which is discretized by multiple finite elements

N_y, respectively, see Fig. 1b. A larger N means smaller partitions and larger design space with more degrees of freedom, while in the Z-direction, the user can specify the number of finite elements used to discretize the lattice height, denoted by N_z.

A given ground lattice structure layout sets the length of each lattice cell wall in the design domain, leaving its thickness to be determined through optimization. Therefore, contrary to TO applied to solid structures, where the design variables are material densities of the finite elements, the design variables in LatticeOPT are the thicknesses of lattice cell walls. A single cell wall in a lattice is highlighted in blue in Fig. 1b and is discretized by multiple finite elements. In addition, typical TO frameworks penalize material densities using either the SIMP or RAMP schemes to avoid the presence of intermediate density values (Rozvany 2009), while in the present framework, no penalty scheme is needed. Wall thickness can be regarded as a continuous variable, and any intermediate thickness values within a reasonable range $[t_{min}, t_{max}]$ are physically meaningful and manufacturable via additive manufacturing techniques such as selective laser melting (Frazier 2014). We would like to emphasize that, although the process of varying the shell element thickness is similar to a sizing optimization and/or topometry optimization (Leiva 2004) since LatticeOPT usually involves many more design variables and it alters the cross-section topology directly by removing walls below a minimum thickness, this is still considered to be a topology optimization framework. The use of the term topology optimization is also consistent with many previous studies on the optimization of thin-walled shell structure cross sections that focus on updating shell thickness and removing cell walls below a thickness threshold (Hunkeler et al. 2013; Hunkeler 2014; Duddeck et al. 2016).

2.2 Thickness update schemes

Many previous heuristic TO frameworks for thin-walled structures evolve the design by iteratively updating the lattice wall thicknesses through some predetermined, intuition-based update rules. The central idea embedded in these rules is the homogenization of certain field variables such as stress (Gurdal and Tatting 2000), internal energy density (Hunkeler 2014; Hunkeler et al. 2013; Forsberg and Nilsson 2007; Guo et al. 2011), and strain energy density (Tovar et al. 2006). In the context of increasing the SEA of the lattice, it is intuitive to homogenize the specific energy absorption of each lattice wall (Hunkeler et al. 2013). Inspired by the idea of homogenization of specific energy absorption, we propose two different thickness update schemes; the following sections discuss each in detail.

2.2.1 Scheme 1

Let $\boldsymbol{t}^i$ and $\boldsymbol{E}^i$ be the array of current lattice wall thicknesses and the wall-wise energy absorption, where the superscript i denotes the design iteration index. The jth entry in $\boldsymbol{t}^i$ and $\boldsymbol{E}^i$

denote the wall thickness and current energy absorption of the *jth* lattice cell wall, respectively. In the most general case, the energy absorption array $\boldsymbol{E}^i$ includes the contribution from the stored elastic strain energy and energy dissipated due to plasticity and damage. We define the area-based specific energy absorption Q_j^i (the subscript j denotes the *jth* lattice wall) as:

$$Q_j^i = \frac{E_j^i}{t_j^i L_j}, \tag{1}$$

where L_j denotes the length of the *jth* lattice wall (which does not change with design iterations). Note that we used an area-based definition for SEA instead of a volume-based one since all walls share a constant height. Using the above definition, homogenization of wall-wise SEA is mathematically equivalent to the following optimization problem:

$$\min_{\forall t_j^{i+1}>0} \ \text{std}(\boldsymbol{Q}^{i+1}), \tag{2}$$

where the elements of $\boldsymbol{Q}^{i+1}$ are given by Eq. (1). In the case of a uniform energy density distribution, the standard deviation attains its global minimum of 0. However, Eq. (2) offers little value in practice: $\boldsymbol{E}^{i+1}$ (which is needed to calculate $\boldsymbol{Q}^{i+1}$) is not known *a priori*, nor can it be estimated to first order using a truncated Taylor series given a thickness change array $\Delta\boldsymbol{t}$:

$$\boldsymbol{E}^{i+1} \approx \boldsymbol{E}^i + \boldsymbol{J}^i \Delta \boldsymbol{t}\,, \tag{3}$$

where the components of the Jacobian matrix are given by $J_{pq}^i = \frac{\partial E_p^i}{\partial t_q^i}$. In general, it is difficult to obtain the Jacobian matrix through the adjoint method since the FE tangent stiffness matrix (which is needed in the calculation of the adjoint vector) is not always available from commercial FE packages, and for explicit dynamic simulations, the tangent stiffness matrix is simply not formed. The sheer size of the Jacobian matrix (N_w^2 entries for a model with N_w lattice walls) also makes it prohibitively expensive to estimate using the finite difference method. Therefore, we modify the optimization problem using a zeroth order estimate for $\boldsymbol{Q}^{i+1}$, denoted as $\tilde{\boldsymbol{Q}}^{i+1}$:

$$\tilde{Q}_j^{i+1} = \frac{E_j^i}{t_j^{i+1} L_j}. \tag{4}$$

$\tilde{\boldsymbol{Q}}^{i+1}$ is used in Eq. (2) in place of $\boldsymbol{Q}^{i+1}$. Note that now the only unknowns are the updated thickness array $\boldsymbol{t}^{i+1}$, and the gradient of the scalar objective function is straightforward ($\boldsymbol{E}^i$ is independent of $\boldsymbol{t}^{i+1}$). This is beneficial, as gradient-based optimizers can be employed to efficiently reduce the objective function, which is highly urged in the famous forum paper (Sigmund 2011). For practical purposes, we further require the following variable bounds, volume, and thickness change constraints:

$$t_j^{i+1} \in [t_{min}, t_{max}], \ \forall j = 1, 2, ..., N_w \tag{5}$$

$$\sum_{j=1}^{N_w} t_j^{i+1} L_j - \frac{V^*}{H} = 0, \tag{6}$$

$$||\boldsymbol{t}^{i+1} - \boldsymbol{t}^i||_\infty \leq \Delta t_{max}, \tag{7}$$

where N_w, V^*, and H denote the number of lattice walls, target volume, and lattice height, respectively. In practice, the maximum thickness change constraint (Eq. 7) is converted to bounds on the design variables $\boldsymbol{t}$ during the optimization. Eqs. (4)–(7) define a nonlinear constrained optimization problem, the solution to which provides the updated thickness distribution $\boldsymbol{t}^{i+1}$ in the next design iteration.

2.2.2 Scheme 2

The second update scheme is inspired by the bi-directional evolutionary structural optimization (BESO) method, pioneered by Huang and Xie (2007). It is a heuristic TO method typically applied to solid structures, where each element in the mesh is ranked by a so-called sensitivity number, and elements are added or removed based on their relative sensitivity ranking. When optimizing for SEA, the sensitivity α_j^i at iteration i for element j is defined as (Huang et al. 2007):

$$\alpha_j^i = \frac{V_j}{V_{tot}} - \frac{E_j^i}{E_{tot}^i}, \tag{8}$$

where V_j and E_j^i denote the undeformed volume (remains constant through design iterations) and absorbed energy of the *jth* finite element, respectively. V_{tot} and E_{tot}^i denote the total volume and energy absorption summed over all finite elements in the mesh. Following this definition, we can analogously define the sensitivity for lattice wall j at design iteration $i+1$ as:

$$\alpha_j^{i+1} = \frac{t_j^{i+1} L_j}{\sum_{j=1}^{N_w} t_j^{i+1} L_j} - \frac{E_j^{i+1}}{\sum_{j=1}^{N_w} E_j^{i+1}}. \tag{9}$$

Homogenization of energy density can again be expressed as minimizing the standard deviation of the lattice wall sensitivity number. We define a zeroth-order estimate for $\boldsymbol{\alpha}^{i+1}$, denoted as $\tilde{\boldsymbol{\alpha}}^{i+1}$, by replacing E_j^{i+1} in Eq. (9) by E_j^i, identical to the approximation made in Eq. (4). Then, the second update scheme can be stated in terms of $\tilde{\boldsymbol{\alpha}}^{i+1}$ as:

$$\min_{\forall t_j^{i+1} > 0} \ \text{std}(\tilde{\boldsymbol{\alpha}}^{i+1}), \tag{10}$$

subject to the same bounds and constraints as defined in Eqs. (5)–(7).

2.3 Implementation

The workflow of the LatticeOPT framework is summarized in Alg. (1). To begin the analysis, the user supplies the design space dimensions and the number of lattice cell walls. The user also needs to provide information about the material properties, loading, and boundary conditions (BCs) in the form of a FE input file compatible with the analysis package of choice. For this work, we have selected Abaqus (SIMULIA 2020) to be the analysis tool, but we emphasize that the LatticeOPT framework can work with any other FE packages so long as the user provides a compatible FE input file. A linear thickness scaling is applied to the initial thickness distribution to satisfy the volume constraint directly (lines 1-2). A uniform mesh of the ground lattice structure containing all lattice walls in the system is generated and added to the FE input file (line 3).

With all the preparation work done, we begin the optimization. The current thickness array $\boldsymbol{t}^i$ is added to the input file, from which a FE simulation is conducted, and the wall energy array $\boldsymbol{E}^i$ is calculated (lines 6-7). To measure the performance of the current design, we compute the mass-based SEA, defined as:

$$SEA = \frac{\sum_{j=1}^{N_w} E_j^i}{\rho V^i}, \tag{11}$$

where ρ is the material density. The structure SEA is evaluated using the last output step from the FE simulation. Following the recommendation in Huang and Xie (2008), we average the wall energy array in the current iteration with that from the previous iteration to stabilize the evolution (line 10). However, we do not apply filtering to the energy array to counter checker-boarding as it is commonly done in density-based TO. This is because the absorbed energy of a lattice wall is the sum of all finite elements contained in the wall, which already includes contributions from neighboring elements. Thus, $\boldsymbol{E}^i$ is expected to be less prone to checker-boarding, and no additional filtering is applied. Before solving the optimization problem, we set the variables' bounds based on their current values and the maximum allowable thickness change per iteration, as well as the range of allowable thicknesses (line 12). To solve the nonlinear optimization problem resulted from the thickness update scheme (line 13), we used the *minimize* function from Scipy (Virtanen et al. 2020), and in particular, the trust region constrained algorithm (trust-constr) (Conn et al. 2000; Byrd et al. 1987). It is worth noting that different nonlinear optimizers were tested, such as the sequential least-squares programming (SLSQP), the interior point method (IPOPT) (Biegler and Zavala 2009), and the method of moving asymptotes (MMA) (Svanberg 1987). It was found that IPOPT and trust-constr gave a similar computational performance and were more robust than other methods tested. The trust-constr method was selected for its performance and the advantage that it is a built-in package in Scipy, which is a widely used Python package.

To ensure that the generated designs are manufacturable, we remove walls whose thickness falls below the threshold t_{min} (lines 14–16). Similar to the soft-kill BESO method (Yang et al. 1999), we assign a small thickness (10^{-6} mm) to those 'removed' walls, instead of actually removing them from the FE model. After wall removal, a linear thickness scaling is again applied to ensure that the thresholded design also satisfies the volume constraint (lines 17–18). Finally, the algorithm checks for convergence by monitoring the maximum thickness change (line 20), and moves on to the next design iteration if convergence is not achieved (line 22). We emphasize that the convergence is based on the thickness array, not on the output SEA value of the structures. This is because being a purely heuristic algorithm, LatticeOPT provides no rigorous guarantee for convergence of structure SEA to a local maximum as is the case for other gradient-based TO methods, nor does it guarantee the monotonic increase in structure SEA as more design iterations are completed. Thus, it is difficult to judge convergence based on the output SEA, and we have chosen to judge convergence by the absolute change in wall thickness distribution.

Algorithm 1: LatticeOPT

Input: $[N_x, N_y, N_z]$, $[L, W, H]$, loading, BCs , material properties, max design iteration , Update scheme , $[\boldsymbol{t}^0, t_{min}, t_{max}]$, V^* , Δt_{max}

Output: Optimized design defined by thickness distribution array $\boldsymbol{t}^*$

/* Initialization */

$V^0 \leftarrow H \sum_{j=1}^{N_w} t_j^0 L_j$ // Initial volume

$\boldsymbol{t}^0 \leftarrow \frac{V^*}{V^0} \boldsymbol{t}^0$ // Scaling to satisfy volume constraint

Write FE input file for ground lattice structure

$i \leftarrow 0$

/* Begin optimization */

while $i <$ *max design iteration* **do**

  Add $\boldsymbol{t}^i$ information to FE input file

  Run FE simulation, obtain $\boldsymbol{E}^i$

  Compute mass-based SEA using Eq. (11)

  if $i > 0$ **then**

    $\boldsymbol{E}^i \leftarrow \frac{1}{2}(\boldsymbol{E}^{i-1} + \boldsymbol{E}^i)$ // Average energy with last iteration

  for $j = [1 : N_w]$ **do**

    /* Set variable bounds */

    $bnd_j = [\, max(0, t_j^i - \Delta t_{max}) \,,\, min(t_j^i + \Delta t_{max}, t_{max}) \,]$

  Solve optimization problem using optimizer to update thickness

  for $j = [1 : N_w]$ **do**

    if $t_j^{i+1} < t_{min}$ **then**

      $t_j^{i+1} = 10^{-6}$ // Threshold lattice wall thickness

  $V^{i+1} \leftarrow H \sum_{j=1}^{N_w} t_j^{i+1} L_j$ // Current volume

  $\boldsymbol{t}^{i+1} \leftarrow \frac{V^*}{V^{i+1}} \boldsymbol{t}^{i+1}$ // Scaling to satisfy volume constraint

  Save $\boldsymbol{E}^i$, $\boldsymbol{t}^{i+1}$ to file

  /* Check convergence */

  if $||\boldsymbol{t}^{i+1} - \boldsymbol{t}^i||_\infty < 10^{-2}$ **then**

    break

  $i \leftarrow i + 1$ // Move to next design iteration

3 Results and discussion

In this section, we present three numerical examples that showcase the capabilities of LatticeOPT. In the first example, we performed a benchmark test against the HCA framework developed by Hunkeler et al. (2013), as well as the commercial TO package LS-OPT (Goel et al. 2009) studied therein. In the second example, we optimize a lattice-reinforced beam subjected to three-point bending with a rigid pole, similar to that studied in Zeng and Duddeck (2017). In the last example, we performed optimization of a square lattice sandwiched between two face sheets, subjected to a blast loading. In all examples, the objective of the optimization is to increase the SEA of the structure compared to its initial design. All simulations presented in this section were conducted in Abaqus/Explicit (SIMULIA 2020) on an Intel i7-11800H processor using 8 cores.

Table 1 Piece-wise linear hardening curve used in the work of Hunkeler (2014)

Flow stress (MPa)	180.0	190.0	197.0	211.5	225.8	233.6	238.5	248.5
Equivalent plastic strain	0.0	0.01	0.02	0.05	0.1	0.15	0.2	0.4

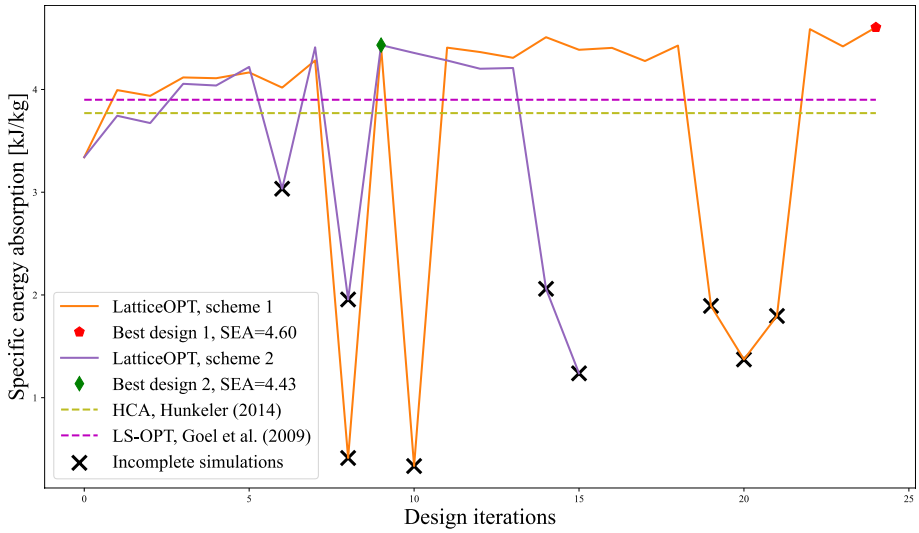

Fig. 2 Evolution history of specific energy absorption in the axial impact case. Both update schemes yield an optimized structure that has a higher specific energy absorption than the HCA and LS-OPT methods. Note that the energy absorption for the incomplete simulation cases (marked with an ×) is lower, as the values of the objective function were computed using the last converged time step and should not be considered as a fair measure of the design performance

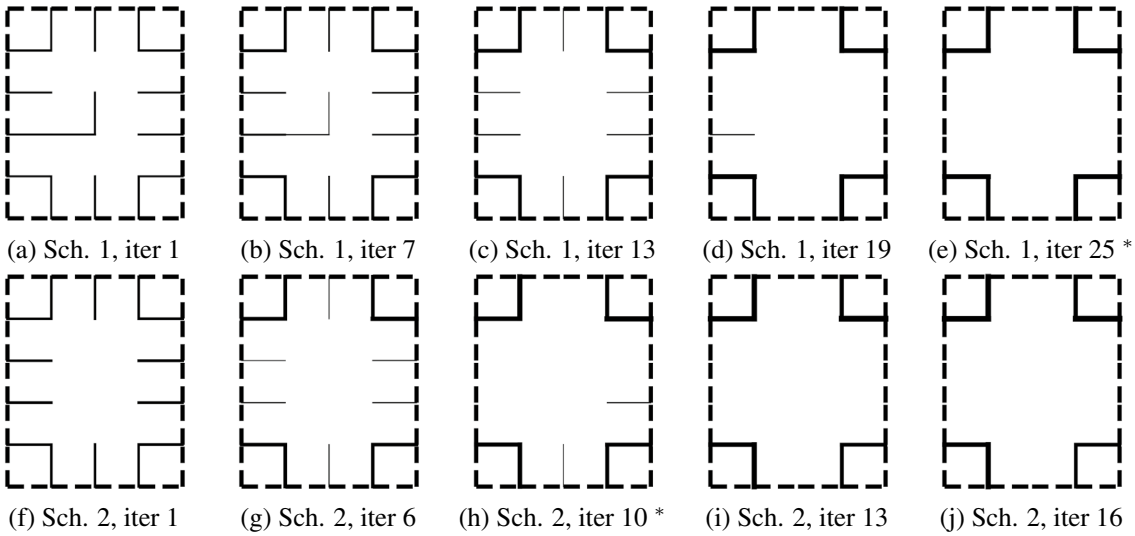

Fig. 3 Designs generated by two update schemes (denoted by Sch in figure captions) at different design iterations; the optimized design that gives the highest specific energy absorption is marked with the superscript *. The line thickness is assigned based on lattice wall thickness; non-designable boundary walls are marked as dashed lines

3.1 Benchmark test against HCA and LS-OPT

Hunkeler (2014) studied the TO of a long, slender column under dynamic axial compression using an HCA-based algorithm. The column has a cross-sectional dimension of 80-by-100 mm^2, and a height of 400 mm. The out-most rectangular boundaries of the column are non-designable and have a fixed wall thickness of 1.5 mm. The cross section is partitioned into 4 cells in the X-direction and 5 cells in the Y-direction, leading to a total of 31 designable lattice walls. However, symmetry boundary conditions were used in Hunkeler (2014), so only a quarter of the cross section with a total of 10 designable walls was included. The material was aluminum with elastoplastic constitutive behavior represented by a rate-independent Mises plasticity model with a piece-wise linear isotropic hardening curve. The hardening curve is provided in Table 1, which was taken from the data in Hunkeler (2014) (see Table 5.4 therein). The column was fixed at the bottom and was subjected to compression by a rigid plate having an initial downward velocity of 5 m/s and a mass of 500 kg. To ensure comparability of results, mesh sizes identical to those in Hunkeler (2014) were used to discretize the structure.

The original optimization problem studied in Hunkeler (2014) was to minimize the mass of the structure while maintaining an end displacement of less than 75 mm after 25 ms. However, the author did report structure SEA at 10 ms for

the optimized designs generated by HCA and LS-OPT (see Table 5.5 therein). As LatticeOPT focuses on optimizing for specific energy absorption instead of controlling end displacement, we reformulated the optimization problem to maximize SEA at 10 ms, subject to a structure mass constraint of 870 g. This target mass is comparable to that of the optimized designs from HCA and LS-OPT, which have masses of 878 and 863 g, respectively (see Table 5.5 therein). Two different TO runs were completed, one with each update scheme presented in Sect. 2.2, and the maximum allowable iterations were set to 25. The minimum and maximum allowable thicknesses were set to 0.4 mm and 2 mm, respectively.

To confirm the comparability of results, the trivial design with only the out-most boundary walls present was simulated, and SEA at 10 ms was found to be 2.09 kJ/kg, very comparable to the 2.01 kJ/kg originally reported in Hunkeler (2014). The small difference can be attributed to the use of symmetry boundary conditions in Hunkeler (2014), which resulted in a slightly different deformation. When using a convergence tolerance of 0.01 mm (see line 20 of Alg. (1)), thickness update scheme 1 did not converge on a design and ran the full 25 design iterations, while update scheme 2 converged after 16 iterations. The evolution histories of SEA for both update schemes are shown in Fig. 2. For reference, we also plot the optimized SEA values from HCA and LS-OPT as reported by Hunkeler (2014) (see Table 5.5 therein). Selected intermediate designs generated by both schemes at different iterations are shown in Fig. 3.

From the evolution history in Fig. 2, we see that neither of the thickness update schemes guarantees the monotonic increase in the objective function value, which is to be expected as the framework is purely heuristic with no rigorous guarantee for convergence to a local optimum. We also note that due to the large deformation nature, not all the simulations were completed successfully, which are marked by a black × in Fig. 2. In the case of a failed simulation, $\boldsymbol{E}$ is simply extracted from the last output step, which corresponds to a smaller load magnitude compared to the full applied load and hence the lower SEA value. Since the SEA value depends not only on the structure design but also on the current load magnitude when its value is calculated, a lower SEA value for failed simulation is *not* necessarily

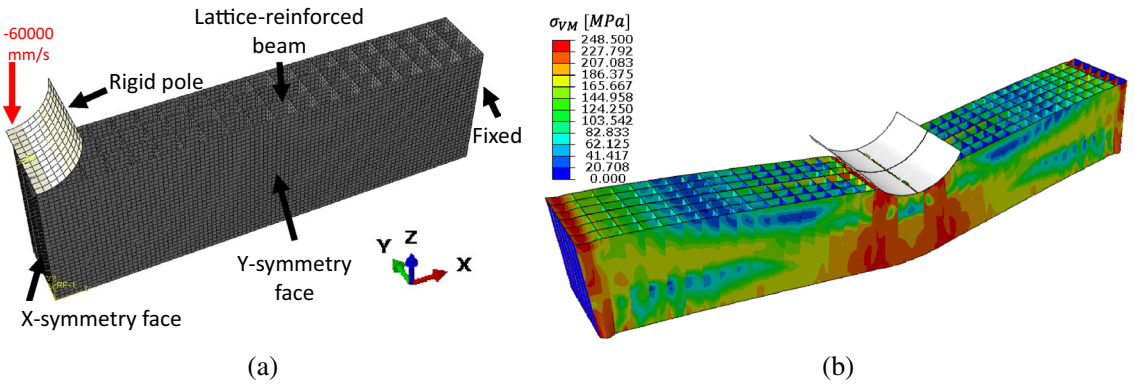

Fig. 4 FE model setup and deformation: **a** The quarter beam model with applied boundary conditions. **b** The deformed initial beam at the end of the simulation, colored by the von Mises stress

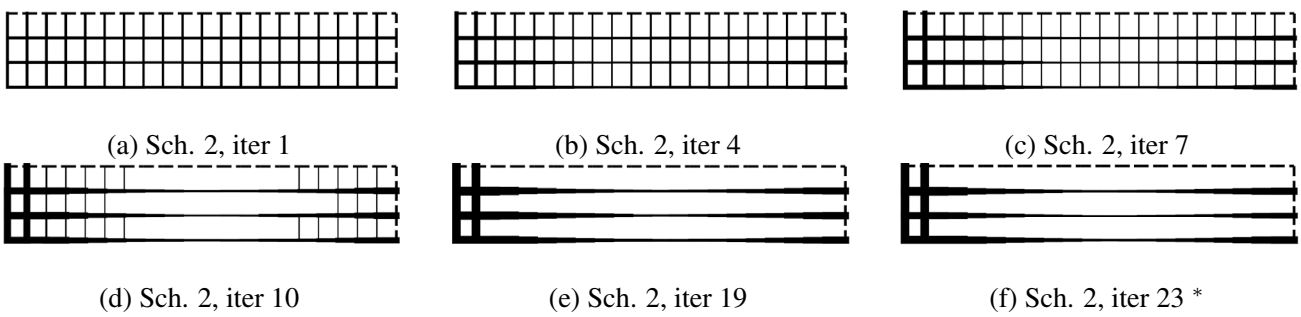

Fig. 5 Designs generated by update scheme (denoted by Sch in figure captions) 2 at different design iterations for the beam example; the optimized design that gives the highest specific energy absorption is marked with the superscript *. Only a quarter of the design cross section is plotted due to symmetry. The line thickness is assigned based on lattice wall thickness; non-designable boundary walls are marked as dashed lines

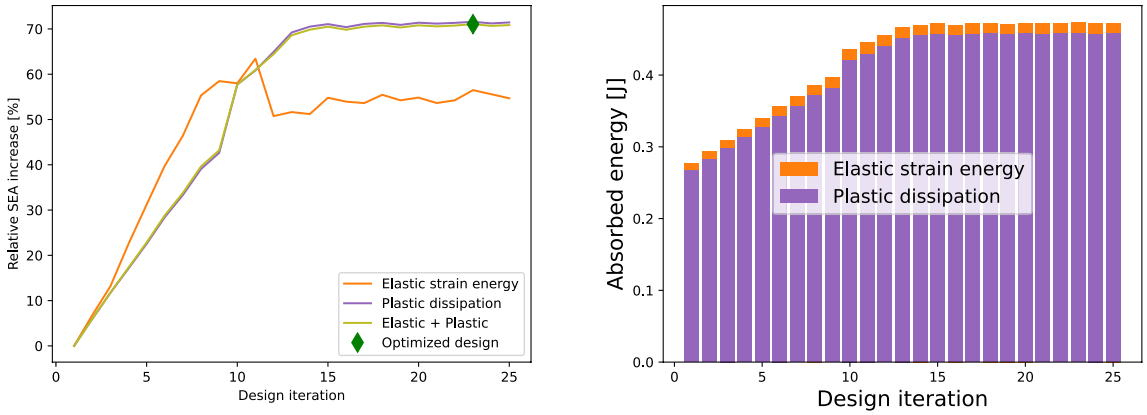

(a) (b)

Fig. 6 Performance evaluation for the dynamic three-point bending case: **a** Relative change in specific energies, normalized by their initial values. **b** Bar chart showing the composition of the total energy absorption into elastic and plastic portions. Note that plastic dissipation is close to the total energy absorption, indicating that plasticity is the primary energy absorption mechanism. The optimized design shows an over 70% increase in SEA compared to the initial design

an indication of a design with poor performance. Despite the oscillatory evolution history, we see that both update schemes produced an optimized design that has higher SEA than the best designs from HCA and LS-OPT.

From Fig. 3, we see that both update schemes quickly removed lattice walls near the center of the column. As the optimization progressed, lattice walls on the four corners of the rectangular column were thickened, and this trend continued to the end of the optimization, where they became the only remaining lattice walls in the designable space. This design feature is consistent with the best designs generated from HCA (see Figure 5.35 therein) as well as LS-OPT (see Figure 5.41 therein) in the work of Hunkeler (2014). The trend where the corner walls get strengthened is also consistent with the findings described in the work of Kim (2002), which found this to be an effective strategy for increasing SEA. We also note that our generated designs are asymmetric due to the lack of symmetry boundary conditions, but this is considered more realistic as a long, slender column tends to buckle in compression, thus breaking the plane of symmetry. The larger design space (31 walls in our case vs. 10 in Hunkeler (2014)) is likely the reason for the higher SEA of the optimized designs generated from LatticeOPT.

Finally, it is worth highlighting the effectiveness of LatticeOPT: both update schemes were able to generate high SEA designs with 25 or fewer FE simulations. As a comparison, the best HCA design was found after 84 simulations, and the best LS-OPT design after 187 simulations. The ability of LatticeOPT to generate optimized designs effectively is vital when the design space is large and results in an expensive FE simulation.

3.2 Optimization of a lattice-reinforced beam under dynamic three-point bending

In the second example, we consider a rectangular beam with a length of 400 mm and a width and height of 60 mm. The beam is fixed at its left and right ends and is subjected to impact with a rigid pole whose radius is 20 mm. The pole travels downward along the height direction of the beam at a fixed velocity of 60000 mm/s for a displacement of 30 mm. The applied boundary conditions are shown in Fig. 4a. We placed 40 and 6 lattice cells along the length and width

Table 2 Material parameters for Johnson-Cook plasticity and damage models, Wang and Shi (2013)

Johnson-Cook plasticity model					
Name	Yield stress (MPa)	Hardening coefficient (MPa)	Strain hardening exponent	Strain rate constant	Thermal softening exponent
Value	1098	1092	0.93	0.014	1.1
Johnson-Cook damage model					
Name	d_1	d_2	d_3	d_4	d_5
Value	− 0.09	0.27	0.48	0.014	3.87

directions, respectively. The out-most rectangular boundaries of the beam cross section are non-designable and have a fixed wall thickness of 0.75 mm. Due to the symmetry of the problem, only a quarter of the domain was modeled with 120 designable walls. The material was identical to that in Sect. 3.1. The initial, minimum, and maximum wall thicknesses were 0.75, 0.4, and 2 mm, respectively. 25 design iterations were conducted using thickness update scheme 2 (see Eq. (10)) to improve the SEA of the beam. The deformed shape of the initial beam design is shown in Fig. 4(b).

The intermediate designs generated during optimization are shown in Fig. 5. In this case, the energy absorbed by the lattice walls has two portions, one from the stored elastic strain energy, and the other from plastic dissipation. We show the relative percent increase in elastic, plastic, and total SEA of the structure in Fig. 6a and detailed composition of energies in Fig. 6b.

Figure 5 shows that the thickness update scheme quickly removed the vertical lattice walls except for those near the rigid pole. This is reasonable as the beam is undergoing transverse loading, whose loads are better carried by horizontal wall elements. The thickness update scheme also generates gradated wall thickness, which is thicker near the center and at the fixed ends, and thinner in the intermediate regions. This design feature is similar to that observed in the work of Zeng et al.(2017), where the HCA-based framework generated lattice fillings with decreasing wall thickness moving away from the beam center (see Figures 11, 12, 13 therein). The thickness update scheme also approached an optimized design fairly quickly: the designs remain very similar after about 15 iterations, which again shows the effectiveness of the LatticeOPT framework. From Fig. 6a, we see an almost monotonic increase in structure SEA with design iterations, with iteration 23 giving the design with the highest SEA. This result shows that the update scheme is highly effective, but the almost monotonic increase in objective function value should not be taken for granted. This finding is merely a coincidence and will not, in general, occur in every case, as the LatticeOPT framework is purely heuristic. But nonetheless, it is shown that the optimized design improved the total SEA by over 70%, and the specific elastic energy storage by over 50%, as compared to the initial design with uniform wall thickness. Figure 6b shows the composition of the total absorbed energy. It is obvious that plastic dissipation is the main mechanism for energy absorption in shell structures, while elastic strain energy only plays a minor role. The total SEA of the structure is improved primarily by increasing the energy absorbed due to plasticity.

3.3 Optimization of a lattice-filled sandwich panel under blast loading

In the last example, a square lattice with a side length of 100 mm and a height of 8.5 mm was considered. Two square face sheets with a side length of 105 mm and a thickness of 2.5 mm were placed on the top and bottom ends of the lattice, and perfect bonding was assumed between the lattice core and face sheets. The assembly was held fixed at the outer region defined by an offset width of 6.07 mm. Taking the center of the face sheet as the origin, 40 g of trinitrotoluene (TNT) was placed at a position (15,15) mm with a stand-off distance of 19 mm from the top surface of the top face sheet. The blast loading generated by the TNT was modeled using the CONWEP model (Randers-Pehrson and Bannister 1997), and the simulation duration was 0.1 ms. The material of all components was Ti-6Al-4V. Due to the complex and dynamic nature of the applied loading, we used the rate-dependent Johnson-Cook plasticity and damage models to capture its material behavior. Key parameters for the model were adapted from the work of Wang and Shi (2013) (see Table 2 therein), and are presented in Table 2. Figure 7a depicts the applied BCs and loads.

The lattice cross section was partitioned into 14 cells in the X- and Y-directions and the out-most boundaries were non-designable with a constant thickness of 0.5 mm. The initial thickness distribution is a uniform wall thickness of 0.25 mm. 25 design iterations were conducted using update scheme 1 (see Eq. (4)) with an objective to increase SEA of the lattice core. Figure 7b depicts the deformation and equivalent stress distribution on the initial lattice design at the end of the simulation.

The thickness update scheme 1 did not converge within the 0.01 mm design tolerance and ran the full 25 design iterations. The design at iteration 22 gave the highest core SEA. The intermediate designs are shown in Fig. 8. Since the material model in this example includes damage, the total absorbed energy has contributions from elastic strain energy, plastic dissipation, and damage dissipation. The percent increase in each energy component compared to the initial design is shown in Fig. 9a. Figure 9b provides a bar chart that shows the detailed composition of the total energy absorbed by the lattice core.

From Fig. 8, it is obvious that the thickness update scheme removed the lattice walls connecting the center region and the fixed boundary walls, and instead concentrated mass near the blast center. As the design progressed, we noticed the formation of a gradated structure, where lattice walls closer to the blast center were assigned a larger wall thickness, and wall thickness decreased rapidly moving away from the blast center. Although the final design appears to have two disconnected parts (the fixed boundary walls and the center region), they remain connected through the upper and lower

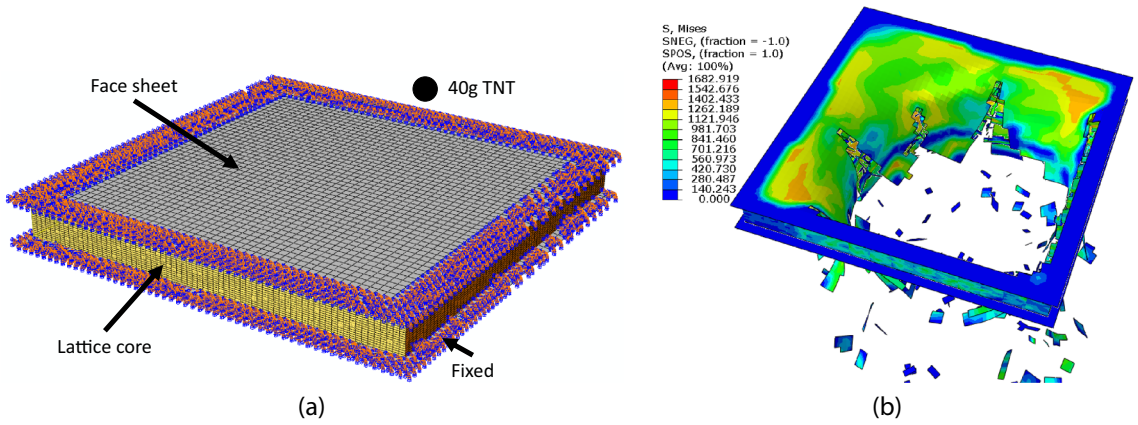

Fig. 7 FE model setup and deformation: **a** Sandwich panel assembly with applied boundary conditions and loads. **b** The deformed initial lattice design at the end of the simulation, colored by the equivalent stress

face sheets and thus remain a physical and manufacturable design. The optimized design is intuitive, where we expect all the mass to be concentrated at the point of impact and radiate outward from it. Figure 9a confirms the effectiveness of the optimized design, as we see the total SEA of the optimized design increased by over 60% compared to the initial design with uniform wall thickness. Besides the plastic dissipation (which shows a similar trend as the total SEA), both the elastic strain energy and the plastic dissipation increased during optimization, with damage dissipation increasing by over 100% compared to the initial value. Inspecting Fig. 9b, we see that plastic dissipation remains the main mechanism for the lattice core energy absorption. Elastic strain energy storage is the second most prominent mechanism, with damage dissipation being the least important mechanism. This example again highlights the effectiveness of LatticeOPT: in

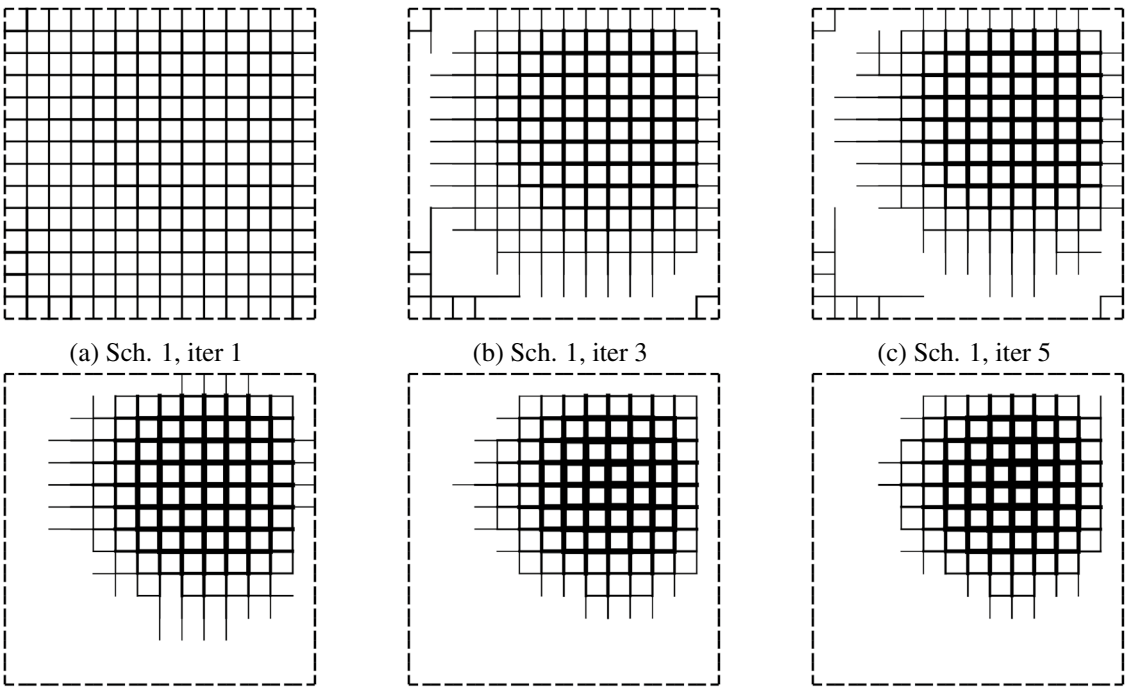

Fig. 8 Designs generated by update scheme (denoted by Sch in figure captions) 1 at different design iterations for the sandwich panel example; the optimized design that gives the highest specific energy absorption is marked with the superscript *. The line thickness is assigned based on lattice wall thickness; non-designable boundary walls are marked as dashed lines

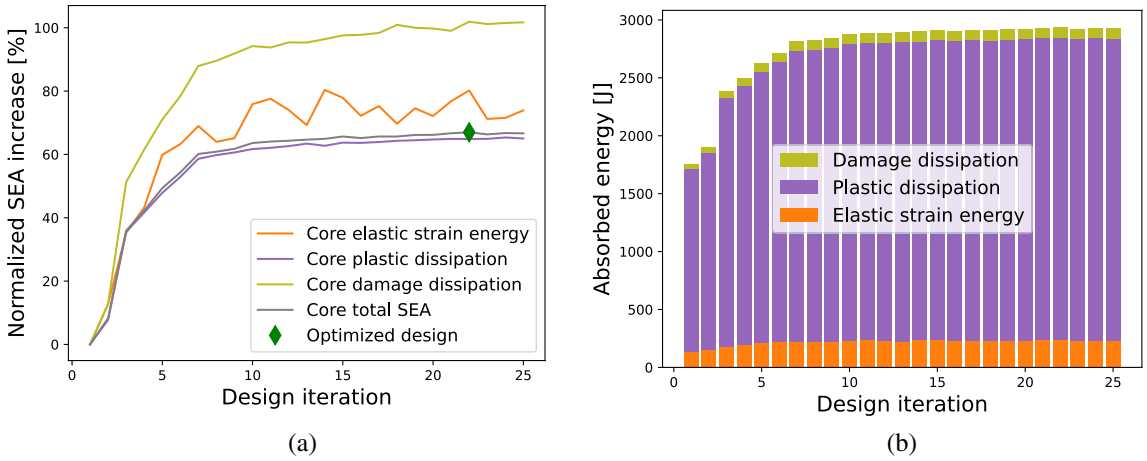

Fig. 9 Performance evaluation for the sandwich panel case: **a** Relative change in specific energies, normalized by their initial values. **b** Bar chart showing the composition of the total energy absorption into elastic, plastic, and damage portions. Note that plastic dissipation is close to the total energy absorption, indicating that plasticity is the primary energy absorption mechanism. The optimized design shows an over 60% increase in SEA compared to the initial design

a case with complex blast loading and a total of 364 designable lattice walls, our framework was able to increase the SEA of the lattice core by over 60% in merely 25 nonlinear FE simulations.

4 Conclusions and future work

In this work, a purely heuristic topology optimization framework to improve the specific energy absorption of thin-walled lattice structures is proposed and tested. The framework relies on a heuristic thickness update scheme that is based on the idea of homogenization of energy density across all lattice walls. Due to its heuristic nature, there is no mathematical guarantee for the monotonic increase in objective function value and for convergence to a local optimum. The thickness update is achieved by solving a nonlinear optimization. Two novel thickness update schemes are presented, one being a direct minimization of the scatter in energy density, and the other is inspired by the BESO method. The framework allows the specification of minimum and maximum allowable wall thicknesses for manufacturing considerations, and lattice walls with thickness below the minimum threshold are removed from the structure. The proposed framework terminates either when the thickness change is below a minimum threshold, or when the maximum number of design iterations is reached.

Three numerical examples are presented to demonstrate the capabilities of the proposed framework. In the first example, we performed a benchmark test with a previous HCA-based topology optimization framework by Hunkeler (2014), where both thickness update schemes were capable of generating designs with higher specific energy absorption than the optimized designs in Hunkeler (2014). We also observed similar design trends in the optimized designs from the current framework and those generated by Hunkeler (2014). In the second example, we optimized a lattice-reinforced beam under dynamic three-point bending. The thickness update scheme was able to effectively increase the specific energy absorption of the beam by over 70%, and a gradated wall thickness distribution was observed. In the last example, we performed topology optimization for a sandwich panel under blast loading, considering material damage behavior. The thickness update scheme quickly concentrated material near the blast center and formed a gradated filling structure where the lattice wall thickness decreases with increasing distance from the blast center. The optimized structure showed an increase in total specific energy absorption by over 60%. In all three presented examples, the proposed framework was able to greatly improve the specific energy absorption of the structure in about 25 design iterations, and in the first example, it is more efficient than the HCA framework proposed in Hunkeler (2014) and the commercial software LS-OPT. Among the three presented examples, thickness update scheme 1 was used in examples 1 and 3, while scheme 2 was used in examples 1 and 2. The purpose of proposing two update schemes is that the user of LatticeOPT has more options if a particular scheme does not yield satisfactory optimization results for the problem at hand. The choice of which scheme to use should be treated the same way as selecting framework parameters, such as the maximum allowable thickness change per iteration. It is an iterative process to determine a set of framework parameters that give the best performance for the given problem.

We conclude that the proposed topology optimization framework can effectively generate thin-walled lattice structures with improved specific energy absorption under different loading conditions. The high effectiveness and the ability to handle complex loading and material behavior render our framework a suitable tool to generate optimized lattice structures for energy-absorbing applications and for improving the crashworthiness of components. One key advantage of this framework is that it does not require the FE stiffness matrix from the FE solver and only needs information on energy absorbed by each finite element. Therefore, with a simple interface, the proposed optimization schemes can be integrated into commercial explicit FE codes to treat highly nonlinear problems. Although all simulations presented in this work were conducted in Abaqus (SIMULIA 2020), the proposed framework can be easily adapted to work with other finite element software.

In future work, we will focus on validating the generated designs through experiments. In addition, the current thickness update schemes employ a zeroth-order estimate for the wall-wise energy during optimization. The work of He et al. (2022) shows the possibility of leveraging a recurrent neural network to predict the energy absorption of the lattice. Similar machine learning models can be applied to increase the prediction accuracy on the wall-wise energy absorption, which will likely accelerate the convergence of the LatticeOPT algorithm and will be the subject of our future work. From the material model perspective, it is known in the literature that the material properties of additively manufactured materials typically depend on the feature size (e.g., wall thickness and strut diameter) (Phutela et al. 2019; Barba et al. 2020; Alghamdi et al. 2021). Therefore, it is of interest to leverage the current framework to study how the size-dependent material properties affect the optimized lattice designs at different length scales.

Acknowledgements We (I. J.) acknowledge the support of the Army Research Office contract (No. W 911NF-18-2-0067) and the National Science Foundation Grant (MOMS-1926353).

Author contributions JH: conceptualization, methodology, software, formal analysis, investigation, datacuration, writing—original draft. SK: methodology, investigation, writing—original draft. DA: supervision, writing—review and editing. IJ: supervision, resources, writing—review and editing, funding acquisition.

Declarations

Conflict of interest The authors declare that they have no conflict of interest.

Replication of results The data and source code that support the findings of this study can be found at: https://github.com/Jasiuk-Research-Group/LatticeOPT.

References

Abramowicz W (2003) Thin-walled structures as impact energy absorbers. Thin-walled Struct 41(2–3):91–107

Abueidda DW, Kang Z, Koric S, James KA, Jasiuk IM (2021) Topology optimization for three-dimensional elastoplastic architected materials using a path-dependent adjoint method. Int J Numer Methods Eng 122(8):1889–1910

Alberdi R, Zhang G, Li L, Khandelwal K (2018) A unified framework for nonlinear path-dependent sensitivity analysis in topology optimization. Int J Numer Methods Eng 115(1):1–56

Alghamdi A, Downing D, Almalki Tino RA, Maconachie T, Lozanovski B, Brandt M, Qian M, Leary M (2021) Buckling phenomena in am lattice strut elements: A design tool applied to Ti-6Al-4V LB-PBF. Mater Des 208:109892

Avalle M, Chiandussi G, Belingardi G (2002) Design optimization by response surface methodology: application to crashworthiness design of vehicle structures. Struct Multidiscipl Optim 24(4):325–332

Barba D, Alabort C, Tang YT, Viscasillas MJ, Reed RC, Alabort E (2020) On the size and orientation effect in additive manufactured Ti-6Al-4V. Mater Des 186:108235

Baroutaji A, Sajjia M, Olabi A-G (2017) On the crashworthiness performance of thin-walled energy absorbers: recent advances and future developments. Thin-Walled Struct 118:137–163

Biegler LT, Zavala VM (2009) Large-scale nonlinear programming using ipopt: an integrating framework for enterprise-wide dynamic optimization. Comput Chem Eng 33(3):575–582

Byrd RH, Schnabel RB, Shultz GA (1987) A trust region algorithm for nonlinearly constrained optimization. SIAM J Numer Anal 24(5):1152–1170

Clausen A, Wang F, Jensen JS, Sigmund O, Lewis JA (2015) Topology optimized architectures with programmable Poisson's ratio over large deformations. Adv Mater 27(37):5523–5527

Conn AR, Gould NIM, Toint PL (2000) Trust region methods. SIAM

Duddeck F, Hunkeler S, Lozano P, Wehrle E, Zeng D (2016) Topology optimization for crashworthiness of thin-walled structures under axial impact using hybrid cellular automata. Struct Multidisc Optim 54(3):415–428

Farrell PE, Ham DA, Funke SW, Rognes ME (2013) Automated derivation of the adjoint of high-level transient finite element programs. SIAM J Sci Comput 35(4):C369–C393

Forsberg J, Nilsson L (2007) Topology optimization in crashworthiness design. Struct Multidisc Optim 33(1):1–12

Frazier WE (2014) Metal additive manufacturing: a review. J Mater Eng Perform 23(6):1917–1928

Gao D, Li X, Chen H (2019) Application of improved particle swarm optimization in vehicle crashworthiness. Math Problems Eng 2019

Goel T, Roux W, Stander N (2009) A topology optimization tool for LS-Dyna users: LS-OPT/Topology. In: 7th European LS-Dyna conference, pp 14–15

Guangyong S, Guangyao L, Shujuan H, Shiwei Z, Wei L, Qing L (2010) Crashworthiness design for functionally graded foam-filled thin-walled structures. Mater Sci Eng A 527(7–8):1911–1919

Guo L, Tovar A, Penninger CL, Renaud JE (2011) Strain-based topology optimisation for crashworthiness using hybrid cellular automata. Int J Crashworth 16(3):239–252

Gurdal Z, Tatting B (2000) Cellular automata for design of truss structures with linear and nonlinear response. In: 41st Structures, Structural Dynamics, and Materials Conference and Exhibit, p 1580

He J, Kushwaha S, Abueidda D, Jasiuk I (2022) Exploring the structure-property relations of thin-walled, 2d extruded lattices using neural networks. arXiv preprint arXiv:2205.06761

Huang X, Xie YM (2007) Convergent and mesh-independent solutions for the bi-directional evolutionary structural optimization method. Finite Elements Anal Des 43(14):1039–1049
Huang X, Xie YM (2008) Optimal design of periodic structures using evolutionary topology optimization. Struct Multidisc Optim 36(6):597–606
Huang X, Xie YM, Lu G (2007) Topology optimization of energy-absorbing structures. Int J Crashworth 12(6):663–675. https://doi.org/10.1080/13588260701497862
Hunkeler S (2014) Topology Optimisation in Crashworthiness Design via Hybrid Cellular Automata for Thin Walled Structures. PhD thesis, Queen Mary University of London,
Hunkeler S, Duddeck F, Rayamajhi M (2013) Topology optimisation method for crashworthiness design using hybrid cellular automata and thin-walled ground structures. In 9th Europ LS-DYNA conf. Manchester
James KA, Waisman H (2015) Topology optimization of structures under variable loading using a damage superposition approach. Int J Numer Methods Eng 101(5):375–406
Jang HAH-H, Lee JY, Park GJ (2012) Dynamic response topology optimization in the time domain using equivalent static loads. AIAA J 50(1):226–234
Jie F, Liu Q, Liufu K, Deng Y, Fang J, Li Q (2019) Design of bionic-bamboo thin-walled structures for energy absorption. Thin-Walled Struct 135:400–413
Jung D, Gea HC (2004) Topology optimization of nonlinear structures. Finite Elements Anal Des 40(11):1417–1427
Kim H-S (2002) New extruded multi-cell aluminum profile for maximum crash energy absorption and weight efficiency. Thin-Walled Struct 40(4):311–327
Kurtaran H, Eskandarian A, Marzougui D, Bedewi NE (2002) Crashworthiness design optimization using successive response surface approximations. Comput Mech 29(4):409–421
Lee H-A, Park G-J (2015) Nonlinear dynamic response topology optimization using the equivalent static loads method. Comput Methods Appl Mech Eng 283:956–970
Leiva J (2004) Topometry optimization: a new capability to perform element by element sizing optimization of structures. In: 10th AIAA/ISSMO multidisciplinary analysis and optimization conference, pp 4595
Li L, Zhang G, Khandelwal K (2017) Topology optimization of energy absorbing structures with maximum damage constraint. Int J Numer Methods Eng 112(7):737–775
Liu T, Sun G, Fang J, Zhang J, Li Q (2019a) Topographical design of stiffener layout for plates against blast loading using a modified ant colony optimization algorithm. Struct Multidisc Optim 59(2):335–350
Liu K, Wu T, Detwiler D, Panchal J, Tovar A (2019b) Design for crashworthiness of categorical multimaterial structures using cluster analysis and Bayesian optimization. J Mech Des 141, 1 (12)
Liu J, Wang Y, Sun G, Pang T (2021) Multisurrogate-assisted ant colony optimization for expensive optimization problems with continuous and categorical variables. IEEE Trans Cybern 1:1
Maute K, Schwarz S, Ramm E (1998) Adaptive topology optimization of elastoplastic structures. Struct Optim 15(2):81–91
Murray YD (2007) User's manual for LS-DYNA concrete material model 159. Report no. FHWA-HRT-05-062. USA: US Department of Transportation, Federal Highway Administration National Transportation Systems Center.
Ngoc SH, Guoxing L (2020) Thin-walled corrugated structures: a review of crashworthiness designs and energy absorption characteristics. Thin-Walled Struct 157:106995
Pauli V, Ralf G, Travis EO, Matt H, Tyler R, David C, Evgeni B, Pearu P, Warren W, Jonathan B, van der Walt SJ, Brett M, Wilson J, Millman KJ, Mayorov N, Nelson ARJ, Jones E, Kern R, Larson E, Carey CJ, Polat İ, Feng Y, Moore EW, VanderPlas J, Laxalde D, Perktold J, Cimrman R, Henriksen I, Quintero EA, Harris CR, Archibald AM, Ribeiro AH, Pedregosa F, van Mulbregt P (2020) SciPy 1.0 Contributors. SciPy 1.0. Fundamental Algorithms for Scientific Computing in Python. Nat Methods 17:261–272. https://doi.org/10.1038/s41592-019-0686-2
Phutela C, Aboulkhair NT, Tuck CJ, Ashcroft I (2019) The effects of feature sizes in selectively laser melted Ti-6Al-4V parts on the validity of optimised process parameters. Materials 13(1):117
Randers-Pehrson G, Bannister KA (1997) Airblast loading model for DYNA2D and DYNA3D. Technical report, Army research lab aberdeen proving Ground MD
Rozvany GIN (2009) A critical review of established methods of structural topology optimization. Struct Multidisc Optim 37(3):217–237
SIMULIA. Abaqus, (2020)
Sigmund O (2011) On the usefulness of non-gradient approaches in topology optimization. Struct Multidiscipl Optim 43(5):589–596
Soto CA, Diaz AR (1999) Basic models for topology design optimization in crashworthiness problems. In International Design Engineering Technical Conferences and Computers and Information in Engineering Conference, 19715, pp 1055–1064. American Society of Mechanical Engineers
Sun G, Fengxiang X, Li G, Li Q (2014) Crashing analysis and multi-objective optimization for thin-walled structures with functionally graded thickness. Int J Impact Eng 64:62–74
Suzhen W, Zheng G, Sun G, Liu Q, Li G, Li Q (2016) On design of multi-cell thin-wall structures for crashworthiness. Int J Impact Eng 88:102–117
Svanberg K (1987) The method of moving asymptotes-a new method for structural optimization. Int J Numer Methods Eng 24(2):359–373
Tsay JJ, Arora JS (1990) Nonlinear structural design sensivitity analysis for path dependent problems part 1: General theory. Comput Methods Appl Mech Eng 81(2):183–208
Tovar A, Patel NM, Niebur GL, Sen M, Renaud JE (2006) Topology optimization using a hybrid cellular automaton method with local control rules. J Mech Des 128(6):1205–1216. https://doi.org/10.1115/1.2336251
Verbart A, Langelaar M, van Keulen F (2016) Damage approach: a new method for topology optimization with local stress constraints. Struct Multidisc Optim 53(5):1081–1098
Wallin M, Jönsson V, Wingren E (2016) Topology optimization based on finite strain plasticity. Struct Multidisc Optim 54(4):783–793
Wang X, Shi J (2013) Validation of Johnson-Cook plasticity and damage model using impact experiment. Int J Impact Eng 60:67–75
Yang XY, Xie YM, Steven GP, Querin OM (1999) Bidirectional evolutionary method for stiffness optimization. AIAA J 37(11):1483–1488
Yin H, Wen G, Liu Z, Qing Q (2014) Crashworthiness optimization design for foam-filled multi-cell thin-walled structures. Thin-Walled Struct 75:8–17
Zarei HR, Kröger M (2007) Crashworthiness optimization of empty and filled aluminum crash boxes. Int J Crashworth 12(3):255–264
Zeng D, Duddeck F (2017) Improved hybrid cellular automata for crashworthiness optimization of thin-walled structures. Struct Multidisc Optim 56(1):101–115

Zhu G, Qiang Y, Zhao X, Wei L, Ho Chen (2020) Energy-absorbing mechanisms and crashworthiness design of cfrp multi-cell structures. Compos Struct 233:111631